Single-Atom Catalysis Hot Paper

International Edition: DOI: 10.1002/anie.201509241
German Edition: DOI: 10.1002/ange.201509241

Single-Atom Catalyst of Platinum Supported on Titanium Nitride for Selective Electrochemical Reactions

*Sungeun Yang, Jiwhan Kim, Young Joo Tak, Aloysius Soon, and Hyunjoo Lee**

Abstract: *As a catalyst, single-atom platinum may provide an ideal structure for platinum minimization. Herein, a single-atom catalyst of platinum supported on titanium nitride nanoparticles were successfully prepared with the aid of chlorine ligands. Unlike platinum nanoparticles, the single-atom active sites predominantly produced hydrogen peroxide in the electrochemical oxygen reduction with the highest mass activity reported so far. The electrocatalytic oxidation of small organic molecules, such as formic acid and methanol, also exhibited unique selectivity on the single-atom platinum catalyst. A lack of platinum ensemble sites changed the reaction pathway for the oxygen-reduction reaction toward a two-electron pathway and formic acid oxidation toward direct dehydrogenation, and also induced no activity for the methanol oxidation. This work demonstrates that single-atom platinum can be an efficient electrocatalyst with high mass activity and unique selectivity.*

Platinum (Pt) is one of the most widely used catalytic materials. Because of its high costs and rarity, minimizing Pt usage while maximizing catalytic activity and selectivity has been the focus of much research. The Pt nanostructure and its catalytic properties are highly correlated. Numerous studies have been attempted to control the sizes and exposed facets of the Pt nanoparticles, form core–shell structures with secondary metals, or modulate metal–support interactions.[1]

Recently, single-atom Pt catalysts were successfully prepared, and these catalysts exhibited high catalytic activity. Atomically dispersed Pt species were prepared on a MgO support, and these species were found to be active for propane combustion.[2] Single-atom Pt immobilized on FeO_x has been detected by electron microscopy, and this catalyst exhibited high activity for CO oxidation or nitroarene hydrogenation.[3] Isolated Pt atoms bound to alumina or zeolites are active for CO oxidation.[4] Pt has also been doped into a TiO_2 or MoS_2 surface on the atomic level, and these catalysts exhibited high activity for photocatalytic or electrocatalytic hydrogen-evolution reaction.[5] These single-atom structures received much attention because their structure would maximize Pt atom utilization with a very high activity per Pt unit mass. However, the single-atom nature would also significantly affect the selectivity. Many reactions require Pt ensemble sites where more than two atoms in the reactants are adsorbed together. The ensemble site effect on catalysis was proved experimentally[6] and theoretically.[7] The absence of a Pt ensemble in the single-atom Pt catalyst would substantially change the reaction pathway compared with that of conventional Pt nanoparticle catalysts.

Electrocatalytic reactions have been actively studied because they can provide energy or chemicals in a more environmentally friendly way.[8] In particular, the electrochemical production of hydrogen peroxide using a fuel cell system has received increasing attention.[9] This approach provides a simpler and safer method for the production of hydrogen peroxide from hydrogen and oxygen compared with the conventional Anthraquinone process or a gas-phase reaction. Isolated single-atom Pt active sites are crucial for achieving high selectivity to hydrogen peroxide from the oxygen-reduction reaction.[7b,10] Two adjacent active sites can adsorb an oxygen molecule and eventually break the oxygen-oxygen bond. Conventional Pt nanoparticle catalysts typically follow a $4e^-$ pathway ($O_2+4H^++4e^-\rightarrow 2H_2O$) to produce water upon oxygen reduction. However, isolated Pt would not be able to break the oxygen–oxygen bond, and the reaction would follow a $2e^-$ pathway ($O_2+2H^++2e^-\rightarrow H_2O_2$) to generate hydrogen peroxide. Previous studies prepared isolated atomic Pt sites by covering Pt nanoparticles with a secondary material, such as Hg[10a] or amorphous carbon.[10b] Although the approach that involves covering the Pt nanoparticles exhibited high selectivity for the production of hydrogen peroxide, the mass activity was limited due to the high proportion of occluded Pt atoms. Another interesting example of the change in the reaction pathway involves the electrocatalytic oxidation of small organic molecules. Formic acid oxidation typically follows an indirect dehydration pathway ($HCOOH\rightarrow H_2O+CO_{ads}$) on conventional Pt nanoparticles. However, density functional theory (DFT) calculations and model surface studies have predicted that a single-atom Pt would catalyze formic acid oxidation according to a direct dehydrogenation pathway ($HCOOH\rightarrow 2H^++CO_2$).[6c,7a] We previously demonstrated that atomically dispersed Pt deposited on octahedral Au nanoparticles followed the direct pathway.[11] In addition, Pt nanoparticles covered with Bi adatoms or cyanide ions can catalyze formic acid oxidation following the direct pathway.[6c,12]

In this study, we prepared single-atom Pt supported on TiN nanoparticles. Our previous DFT calculations predicted that a single-atom Pt can be stabilized on a *N*-vacancy site on the TiN support.[13] The isolated Pt atoms were confirmed

[*] Dr. S. Yang, J. Kim, Prof. H. Lee
Department of Chemical and Biomolecular Engineering
Korea Advanced Institute of Science and Technology
291, Daehak-ro, Yuseong-gu, Daejeon 34141 (Republic of Korea)
E-mail: azhyun@kaist.ac.kr
Y. J. Tak, Prof. A. Soon
Department of Material Science and Engineering, Yonsei University
50, Yonsei-ro, Seodaemun-gu, Seoul 03722 (Republic of Korea)

Supporting information for this article is available on the WWW under http://dx.doi.org/10.1002/anie.201509241.

using high-angle annular dark-field scanning transmission electron microscopy (HAADF-STEM) and extended X-ray absorption fine structure (EXAFS) analysis, and these atoms exhibited unique electrocatalytic properties for oxygen reduction, formic acid oxidation, and methanol oxidation.

Single-atom Pt deposited on a TiN support was prepared using the incipient wetness impregnation (IWI) method. When a small amount of Pt as low as 0.35 wt% was loaded onto the support, single-atom Pt was observed but Pt nanoparticles were rarely observed. However, higher amounts of Pt typically generated nanoparticles. Three different weight percentages of Pt were deposited onto the TiN supports (i.e., 0.35, 2, and 5 wt%). Figure 1a shows the

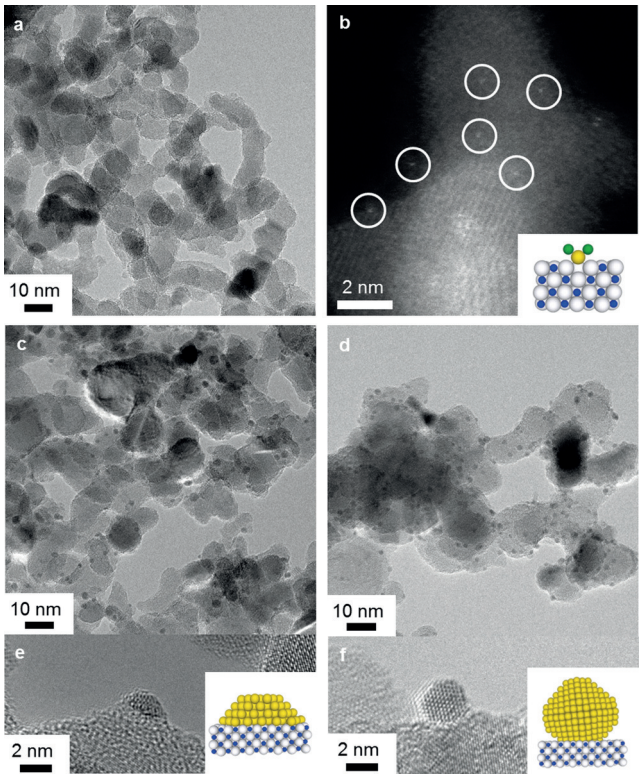

Figure 1. a) TEM and b) HAADF-STEM images of 0.35 wt% Pt/TiN. TEM and HR-TEM images of c,e) 5 wt% Pt/TiN prepared using the IWI method and d,f) 5 wt% Pt NP/TiN prepared using the EG method. Inset models are a schematic representation of each catalyst (Pt; yellow, Ti; white, N: blue, and Cl: green).

TEM image of the 0.35 wt% Pt/TiN sample, and no detectable Pt nanoparticles were observed. Only TiN nanoparticles were observed. However, its HAADF-STEM image, which is shown in Figure 1b, indicated the presence of white points, which are single-atom Pt. Additional HAADF-STEM images are shown in Figure S1 in the Supporting Information. The 5 wt% Pt/TiN sample contained many Pt nanoparticles, as shown in Figure 1c. Its HR-TEM images, which are shown in Figure 1e and Figure S2, revealed many hemispherical Pt nanoparticles spread on the TiN supports. The 2 wt% Pt/TiN sample exhibited intermediate features that consisted of both single-atom Pt and very small Pt nanoparticles, as shown in Figure S3. For comparison, the 5 wt% Pt NP/TiN (Pt nanoparticles on TiN) sample was prepared using the ethylene glycol (EG) method.[14] Here, the Pt nanoparticles were separately prepared in the solution and then deposited on the TiN support. The extent of wetness of the Pt nanoparticles on the TiN supports was less than that of the Pt/TiN sample prepared by the IWI method. The HR-TEM images indicated that the Pt nanoparticles possessed more spherical shapes, as shown in Figure 1f and Figure S4. The particle size was estimated from the TEM images, and the average size of the Pt domain was 2.29 ± 0.63 nm in the 5 wt% Pt/TiN sample and 2.00 ± 0.30 nm in the 5 wt% Pt NP/TiN sample. The commercial Pt/C (20 wt% Johnson–Matthey) has an average size of 2.36 ± 0.50 nm. The size distribution histograms are shown in Figure S5.

While electron microscopy only provides limited information on the specific local area, X-ray absorption spectroscopy analysis can provide more representative information on the overall structure. Figure 2a and c show the EXAFS analysis data, and Table S1 shows the results from EXAFS data fitting. The 0.35 wt% Pt/TiN sample exhibited a strong peak at approximately 2 Å and smaller wiggles at 2–3 Å. The Pt-Cl interaction is responsible for the strong peak at approximately 2 Å, and the smaller wiggles at 2–3 Å are

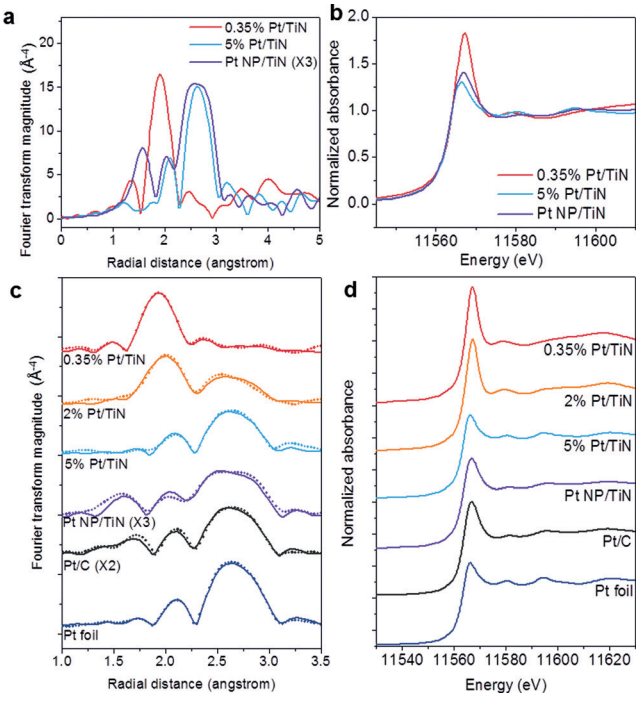

Figure 2. a,c) Pt L3 edge k^3-weighted FT-EXAFS spectra of the samples: 0.35 wt%, 2 wt%, and 5 wt% Pt/TiN prepared using the IWI method, 5 wt% Pt NP/TiN prepared using the EG method, 20 wt% JM Pt/C, and Pt foil. Dots indicate experimental data, and the lines are the fitted results. Magnitude of FT-EXAFS spectra of 20 wt% Pt/C was doubled and 5 wt% Pt NP/TiN was tripled for easier comparison. b,d) Pt L3 edge X-ray absorption near edge structure (XANES) of the samples. Diagrams (a) and (b) show a direct comparison of single-atom Pt catalyst (0.35 wt% Pt/TiN), Pt nanoparticles with a strong interaction with TiN (5 wt% Pt/TiN), and Pt nanoparticles with a relatively weak interaction with TiN (5 wt% Pt NP/TiN).

due to small Pt–Ti and Pt–Pt interactions. The coordination number of the 0.35 wt% Pt/TiN sample was 3.038 for Pt–Cl, 0.583 for Pt–Pt, and 0.573 for Pt–Ti, which indicates that the single-atom Pt was primarily stabilized by chlorine ligands. The Pt–Pt coordination number was much smaller than that of typical Pt nanoparticles, thus confirming the presence of isolated Pt atoms on the TiN support. A small interaction between Pt and Ti was also observed, which indicated the anchoring effect of the TiN surface. The interatomic Pt–Ti distance was theoretically predicted to be 2.66 Å when the Pt atom was located on the N vacancy of the TiN surface without any other ligand;[13b] based on EXAFS data fitting, this value was determined to be 2.713 Å. The experimental value is slightly longer than the theoretical value, which is most likely due to the strong Pt–Cl interaction elongating the Pt–Ti distance. As the weight percentage of Pt increased, the structural feature changed dramatically. The coordination number for Pt–Cl decreased from 3.038 for the 0.35 wt% Pt/TiN sample to 2.640 for the 2 wt% Pt/TiN sample and to 0.166 for the 5 wt% Pt/TiN sample, and the coordination number for Pt–Pt increased from 0.583 for the 0.35 wt% Pt/TiN sample to 3.371 for the 2 wt% Pt/TiN sample and to 8.310 for the 5 wt% Pt/TiN sample. The 2 wt% Pt/TiN sample still contained single-atom Pt along with Pt nanoparticles, and the 5 wt% Pt/TiN sample primarily contained Pt nanoparticles. Interestingly, the 5 wt% Pt/TiN sample did not exhibit any Pt–O interactions that typically appear in Pt nanoparticles at 1.6–1.7 Å. The 5 wt% Pt NP/TiN and 20 wt% Pt/C exhibited the Pt–O interaction with a coordination number of 0.671 and 1.285, respectively. The Pt/TiN sample prepared using the IWI method appears to have a stronger metal–support interaction between Pt and TiN with a more reduced Pt state than that of the Pt NP/TiN sample prepared using the EG method.[14] The stronger interaction most likely resulted in the more wetted form of the Pt nanoparticles that were observed in Figure S2.

The Pt electronic structure was also observed using X-ray absorption near edge structure (XANES) analysis, as shown in Figure 2b and d. The white line peak in the XANES for the Pt L3 edge corresponds to an electronic transition from $2p_{2/3}$ to unoccupied 5d states. A lower white line intensity indicates that the Pt has a more reduced electronic structure. The white line intensity was the highest for the 0.35 wt% Pt/TiN sample, confirming the oxidized electronic structure of the single-atom Pt. Previous studies on single-atom Pt also reported an oxidized electronic structure for Pt.[2,3,4c,5b,15] The white line intensity was much less for Pt nanoparticles supported on TiN or carbon. Consistent with the EXAFS results, Pt/TiN prepared using the IWI method exhibited an even smaller white line intensity than did Pt NP/TiN or Pt/C, which indicated that the Pt was in a more reduced state.

The oxygen-reduction reaction (ORR) was electrochemically performed in an acidic aqueous solution using a rotating ring disk electrode (RRDE). The ORR can follow either of a $4e^-$ or $2e^-$ pathway. Both oxygen atoms of the oxygen molecule need to be adsorbed on surface active sites to dissociate the strong O=O double bond. At least two adjacent active sites are necessary for the $4e^-$ pathway. The isolated single-atom sites would not be able to break O=O bonds, following the $2e^-$ pathway. Figure 3 shows the oxygen

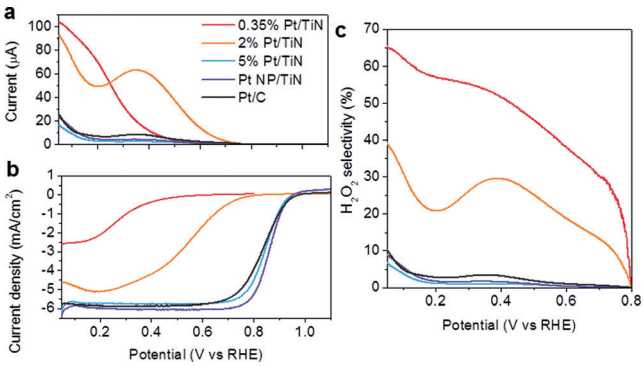

Figure 3. a) Ring currents concurrently obtained during the ORR with a potential maintained at 1.2 V for various samples: 0.35, 2, and 5 wt% Pt/TiN prepared using the IWI method, 5 wt% Pt NP/TiN prepared using the EG method, and 20 wt% JM Pt/C. b) ORR polarization curves in O_2-saturated 0.1 M $HClO_4$ and c) H_2O_2 selectivity calculated from the oxygen reduction current and the H_2O_2 oxidation current.

reduction currents measured on a disk electrode and the H_2O_2 oxidation currents measured on a ring electrode. When the RRDE was rotated, the H_2O_2 produced at the disk electrode was radially transferred to the ring electrode and then oxidized. The H_2O_2 selectivity can be calculated from the ORR and H_2O_2 oxidation currents according to the following equation: H_2O_2 selectivity $(\%) = (2i_R/N)/((i_R/N) + i_D) \times 100$, where i_R is the ring current, i_D is the disk current, and N is the collection efficiency (0.335 for the specific RRDE that we have used). In comparison to the other samples, single-atom Pt (0.35 wt% Pt/TiN sample) exhibited much smaller oxygen reduction currents. However, the H_2O_2 oxidation currents were surprisingly high, and the H_2O_2 selectivity reached 65%. The single-atom active sites were responsible for the high selectivity towards H_2O_2. For the 2 wt% Pt/TiN sample, the oxygen reduction currents increased but the H_2O_2 selectivity decreased significantly to 20–30%. All of the other samples exhibited much higher oxygen reduction currents, but the H_2O_2 selectivity was less than 5%. The 5 wt% Pt/TiN or 5 wt% Pt NP/TiN samples exhibited an even lower H_2O_2 selectivity than that of commercial Pt/C. The 0.35 wt% Pt/TiN sample did not exhibit 100% selectivity for H_2O_2 production, which was most likely due to the presence of a small amount of Pt nanoparticles that can catalyze the $4e^-$ pathway. Although the Pt nanoparticles were barely observed using electron microscopy, the Pt–Pt coordination number of 0.583 might indicate the existence of Pt nanoparticles. The Pt/TiN samples with even lower Pt weight percentages were prepared with 0.1 wt% and 0.05 wt%. These samples are expected to have a higher portion of single-atom Pt than the 0.35 wt% Pt/TiN sample. The H_2O_2 selectivity values of the 0.05 wt% and 0.1 wt% Pt/TiN samples were higher than the 0.35 wt% Pt/TiN sample, reaching as high as 90%. However, oxygen reduction currents were greatly reduced as the number of active sites decreased (Figure S6). Additionally, the TiN support may cleave the O=O bond.[16] The acid-treated TiN we used in this study, however, barely showed the activity for the ORR as shown in Figure S7a.

The activity of various Pt catalysts was compared. The kinetic current was calculated using the Koutecky–Levich equation ($1/i = 1/i_K + 1/i_L$, where i is the measured current, i_K is the kinetic current, and i_L is the diffusion-limiting current) at an overpotential of 0.25 V for two different pathways. Because the kinetic currents contained both pathways to H_2O and H_2O_2, the current was separately calculated. The mass activity was calculated by dividing the kinetic currents towards H_2O_2 (for 0.35 wt% Pt/TiN) or H_2O (for 5 wt% Pt/TiN, Pt NP/TiN, and Pt/C) by the Pt mass, and the specific activity was calculated by dividing the kinetic currents towards H_2O_2 or H_2O by the electrochemically active surface area (ECSA). The ECSA was obtained by averaging the H adsorption and desorption peaks that appeared during cyclic voltammetry that was performed in an Ar-saturated 0.1 M $HClO_4$ solution. Because the 0.35 wt% Pt/TiN sample did not exhibit distinct H adsorption and desorption peaks, its ECSA was calculated based on the assumption that all of the Pt atoms are exposed. Figure 4 shows the comparison. The single-atom Pt (0.35 wt% Pt/TiN) exhibited an order of magnitude higher mass activity than the Pt nanoparticles (5 wt% Pt/TiN, Pt NP/TiN, Pt/C). To the best of our knowledge, the highest mass activity obtained for electrochemical H_2O_2 production is 26 A per gram Pt at an overpotential of 0.05 V.[10a] When the mass activity was estimated at the same overpotential, the single-atom Pt exhibited a record-breaking high mass activity of 78 A per gram Pt. The specific activity of the single-atom Pt was also higher than that for Pt nanoparticles.

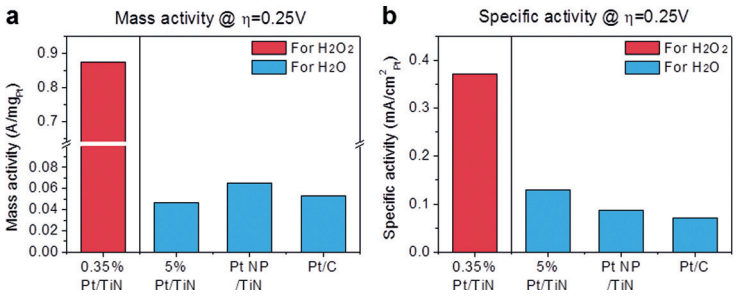

Figure 4. a) Mass activity and b) surface area specific activity of various Pt catalysts. Because the single-atom Pt catalyst (0.35 wt% Pt/TiN prepared by the IWI method) primarily followed the two-electron pathway and the other catalysts (5 wt% Pt/TiN prepared by the IWI method, 5 wt% Pt NP/TiN prepared by the EG method, 20 wt% JM Pt/C) followed the four-electron pathway, the activity was compared at the same overpotential (0.25 V).

The durability of the single-atom Pt catalyst is important for practical applications. A chronoamperometry test was performed to evaluate the durability by holding the potential at 0.3 V. Although the reduction current decreased over time, the selectivity towards H_2O_2 production was constant (Figure S8). The HAADF-STEM image shown in Figure S8b indicates that the single-atom Pt remained after the durability test. The ORR was performed, and the results before and after the durability test were compared. The activity and selectivity exhibited only slight decrease, which indicated that the single-atom Pt possesses good stability.

The formic acid oxidation reaction (FAOR) and methanol oxidation reaction (MOR) have been actively studied as an anodic reaction for fuel cells.[17] These reactions are a good probe for characterizing the nanostructure of electrocatalysts. The FAOR follows either a direct dehydrogenation pathway or an indirect dehydration pathway. The peak for the direct pathway typically appears at 0.6–0.7 V, and the peak for the indirect pathway appears at 0.9–1.1 V. Adsorbed carbon monoxide (CO_{ad}) produced in the indirect pathway is a poisoning species on the Pt surface and oxidized to CO_2 at a high potential. The Pt nanoparticles typically follow the indirect pathway, as shown for Pt/C in Figure S9a. The direct pathway requires only 1–2 Pt atoms but the indirect pathway needs at least 3–4 Pt atoms.[6b,c,7a] Therefore, only the direct pathway would be possible for the 0.35 wt% Pt/TiN sample, and this expected result was truly observed in Figure S9a. The sample exhibited only one peak that corresponded to the direct pathway. The 2 wt% Pt/TiN sample still followed the direct pathway because of the single-atom Pt, and the mass activity was even higher than that of the 0.35 wt% Pt/TiN sample, which was likely due to Pt being in a more reduced state. However, the peak for the indirect pathway appeared at 0.95 V because of the co-existence of Pt nanoparticles. The Pt nanoparticle catalysts (i.e., 5 wt% Pt/TiN, Pt NP/TiN, and Pt/C) exhibited decreased activity, and the peak for the indirect pathway became dominant. Unlike the FAOR, the MOR requires Pt ensemble sites because all of the pathways for methanol oxidation include CO_{ads}. The single-atom Pt would not be able to catalyze methanol oxidation, and this result was truly observed in Figure S9b. The 0.35 wt% Pt/TiN sample barely exhibited an oxidation current. As the Pt content increased, the mass activity for methanol oxidation increased. The Pt nanoparticles formed on the TiN support exhibited higher activity than the Pt/C catalyst. The TiN surface may aid in methanol oxidation because of a bi-functional effect by providing hydroxy species.[13a,18]

In conclusion, a single-atom Pt catalyst was prepared on TiN nanoparticles using the incipient wetness impregnation method, and this catalyst was used for electrochemical oxygen reduction, formic acid oxidation, and methanol oxidation. The 0.35 wt% Pt/TiN had almost exclusively atomic Pt, and produced hydrogen peroxide following the two electron pathway with a record-breaking high mass activity of 78 A per gram Pt at an overpotential of 0.05 V. The single-atom Pt catalyst followed reaction pathways very different from Pt nanoparticles because of the absence of Pt ensembles.

Acknowledgements

This work was financially supported by the Global Frontier R&D Program at the Center for Multiscale Energy System (2011-0031575) and NRF-2015R1A2A2A01004467 through the National Research Foundation of Korea funded by the Ministry of Education, Science and Technology. The experi-

ments at PLS were supported in part by MSIP and POSTECH.

Keywords: electrocatalysis · platinum · selectivity · single-atom catalysts · titanium nitride

How to cite: *Angew. Chem. Int. Ed.* **2016**, *55*, 2058–2062
Angew. Chem. **2016**, *128*, 2098–2102

[1] a) J. Y. Park, G. A. Somorjai, *Top. Catal.* **2008**, *49*, 126–135; b) K. M. Bratlie, H. Lee, K. Komvopoulos, P. D. Yang, G. A. Somorjai, *Nano Lett.* **2007**, *7*, 3097–3101; c) C. Kim, J. G. Oh, Y. T. Kim, H. Kim, H. Lee, *Electrochem. Commun.* **2010**, *12*, 1596–1599; d) S. Alayoglu, A. U. Nilekar, M. Mavrikakis, B. Eichhorn, *Nat. Mater.* **2008**, *7*, 333–338; e) C. M. Y. Yeung, K. M. K. Yu, Q. J. Fu, D. Thompsett, M. I. Petch, S. C. Tsang, *J. Am. Chem. Soc.* **2005**, *127*, 18010–18011.

[2] K. Asakura, H. Nagahiro, N. Ichikuni, Y. Iwasawa, *Appl. Catal. A* **1999**, *188*, 313–324.

[3] a) B. T. Qiao, A. Q. Wang, X. F. Yang, L. F. Allard, Z. Jiang, Y. T. Cui, J. Y. Liu, J. Li, T. Zhang, *Nat. Chem.* **2011**, *3*, 634–641; b) H. Wei, X. Liu, A. Wang, L. Zhang, B. Qiao, X. Yang, Y. Huang, S. Miao, J. Liu, T. Zhang, *Nat. Commun.* **2014**, *5*, 5634.

[4] a) J. D. Kistler, N. Chotigkrai, P. Xu, B. Enderle, P. Praserthdam, C.-Y. Chen, N. D. Browning, B. C. Gates, *Angew. Chem. Int. Ed.* **2014**, *53*, 8904–8907; *Angew. Chem.* **2014**, *126*, 9050–9053; b) J. H. Kwak, J. Z. Hu, D. Mei, C. W. Yi, D. H. Kim, C. H. F. Peden, L. F. Allard, J. Szanyi, *Science* **2009**, *325*, 1670–1673; c) M. Moses-DeBusk, M. Yoon, L. F. Allard, D. R. Mullins, Z. Wu, X. Yang, G. Veith, G. M. Stocks, C. K. Narula, *J. Am. Chem. Soc.* **2013**, *135*, 12634–12645.

[5] a) J. Deng, H. B. Li, J. P. Xiao, Y. C. Tu, D. H. Deng, H. X. Yang, H. F. Tian, J. Q. Li, P. J. Ren, X. H. Bao, *Energy Environ. Sci.* **2015**, *8*, 1594–1601; b) Y. H. Li, J. Xing, X. H. Yang, H. G. Yang, *Chem. Eur. J.* **2014**, *20*, 12377–12380.

[6] a) F. Maroun, F. Ozanam, O. M. Magnussen, R. J. Behm, *Science* **2001**, *293*, 1811–1814; b) A. Cuesta, *J. Am. Chem. Soc.* **2006**, *128*, 13332–13333; c) A. Cuesta, M. Escudero, B. Lanova, H. Baltruschat, *Langmuir* **2009**, *25*, 6500–6507; d) D. Strmcnik, M. Escudero-Escribano, K. Kodama, V. R. Stamenkovic, A. Cuesta, N. M. Markovic, *Nat. Chem.* **2010**, *2*, 880–885; e) A. Cuesta, M. Escudero, *Phys. Chem. Chem. Phys.* **2008**, *10*, 3628–3634; f) A. Cuesta, *ChemPhysChem* **2011**, *12*, 2375–2385.

[7] a) M. Neurock, M. Janik, A. Wieckowski, *Faraday Discuss.* **2008**, *140*, 363–378; b) H. C. Ham, G. S. Hwang, J. Han, S. W. Nam, T. H. Lim, *J. Phys. Chem. C* **2009**, *113*, 12943–12945.

[8] a) B. C. H. Steele, A. Heinzel, *Nature* **2001**, *414*, 345–352; b) H. G. Cha, K. S. Choi, *Nat. Chem.* **2015**, *7*, 328–333.

[9] a) I. Yamanaka, S. Tazawa, T. Murayama, R. Ichihashi, N. Hanaizumi, *ChemSusChem* **2008**, *1*, 988–992; b) I. Yamanaka, S. Tazawa, T. Murayama, T. Iwasaki, S. Takenaka, *ChemSusChem* **2010**, *3*, 59–62.

[10] a) S. Siahrostami, A. Verdaguer-Casadevall, M. Karamad, D. Deiana, P. Malacrida, B. Wickman, M. Escudero-Escribano, E. A. Paoli, R. Frydendal, T. W. Hansen, I. Chorkendorff, I. E. L. Stephens, J. Rossmeisl, *Nat. Mater.* **2013**, *12*, 1137–1143; b) C. H. Choi, H. C. Kwon, S. Yook, H. Shin, H. Kim, M. Choi, *J. Phys. Chem. C* **2014**, *118*, 30063–30070; c) A. Verdaguer-Casadevall, D. Deiana, M. Karamad, S. Siahrostami, P. Malacrida, T. W. Hansen, J. Rossmeisl, I. Chorkendorff, I. E. L. Stephens, *Nano Lett.* **2014**, *14*, 1603–1608.

[11] S. Yang, H. Lee, *ACS Catal.* **2013**, *3*, 437–443.

[12] Q. S. Chen, Z. Y. Zhou, F. J. Vidal-Iglesias, J. Solla-Gullon, J. M. Feliu, S. G. Sun, *J. Am. Chem. Soc.* **2011**, *133*, 12930–12933.

[13] a) R. Q. Zhang, C. E. Kim, B. D. Yu, C. Stampfl, A. Soon, *Phys. Chem. Chem. Phys.* **2013**, *15*, 19450–19456; b) R. Q. Zhang, T. H. Lee, B. D. Yu, C. Stampfl, A. Soon, *Phys. Chem. Chem. Phys.* **2012**, *14*, 16552–16557.

[14] S. Yang, D. Y. Chung, Y. J. Tak, J. Kim, H. Han, J. S. Yu, A. Soon, Y. E. Sung, H. Lee, *Appl. Catal. B* **2015**, *174*, 35–42.

[15] A. Bruix, Y. Lykhach, I. Matolinova, A. Neitzel, T. Skala, N. Tsud, M. Vorokhta, V. Stetsovych, K. Sevcikova, J. Myslivecek, R. Fiala, M. Vaclavu, K. C. Prince, S. Bruyere, V. Potin, F. Illas, V. Matolin, J. Libuda, K. M. Neyman, *Angew. Chem. Int. Ed.* **2014**, *53*, 10525–10530; *Angew. Chem.* **2014**, *126*, 10693–10698.

[16] Y. Z. Dong, Y. M. Wu, M. J. Liu, J. H. Li, *ChemSusChem* **2013**, *6*, 2016–2021.

[17] a) C. Rice, R. I. Ha, R. I. Masel, P. Waszczuk, A. Wieckowski, T. Barnard, *J. Power Sources* **2002**, *111*, 83–89; b) S. Wasmus, A. Kuver, *J. Electroanal. Chem.* **1999**, *461*, 14–31.

[18] M. M. O. Thotiyl, T. Ravikumar, S. Sampath, *J. Mater. Chem.* **2010**, *20*, 10643–10651.

Received: October 2, 2015
Revised: November 11, 2015
Published online: December 28, 2015

